FIELD INDUCED PHASE TRANSITION IN ONE DIMENSIONAL HEISENBERG ANTIFERROMAGNET MODEL STUDIED USING DENSITY MATRIX RENORMALIZATION GROUP

by

PETER GUSTAINIS

B.Sc., The University of Waterloo, 2015

A THESIS SUBMITED IN PARTIAL FULFILLMENT OF THE REQUIREMENTS FOR THE DEGREE OF

MASTER OF SCIENCE

in

THE FACULTY OF GRADUATE AND POSTDOCTORAL STUDIES

(Physics)

THE UNIVERSITY OF BRITISH COLUMBIA

(Vancouver)

April 2017

Abstract

This thesis examines the Heisenberg antiferromagnetic spin chain in one dimension (1D) with a crystal field splitting term and applied magnetic field term. We use theoretical techniques from quantum field theory and conformal field theory (CFT) to make predictions about the excitation spectrum for our model. We then use Density Matrix Renormalization Group (DMRG) numerical techniques to simulate our spin chain and extract the energy spectrum as we vary our crystal field splitting and magnetic field terms. These results are compared and we examine where theoretical calculations accurately describe our system. This work is motivated by recent experimental work done on $SrNi_2Vi_2O_8$by Bera et al. [1] which is a quasi-1D material with weakly coupled spin chains in the bulk. These 1D chains are expected to be described by the Hamiltonian we study in this thesis, and we neglect interchain coupling. We first consider our system where the crystal field splitting term is set to zero, which can be described theoretically using a mapping to the non linear sigma model (NLSM). Near the critical field, it undergoes a Bose condensation transition whose excitation spectrum can be mapped to non-interacting fermions in 1D. We then consider large negative crystal field splitting, and find that near small applied magnetic field we can describe some excited states using Landau-Ginsburg theory. Near critical field, we show that the transition is in the Ising universality, and use results from CFT to predict the spectrum for finite size systems. This allows us to make predictions about where the transition field would be for very large or infinite system size. Finally, we examine our crystal field splitting tuned to the value obtained in Ref. 1, which is a small, negative value. We observe qualitative elements in this spectrum from the spectra obtained at zero and large negative crystal field splitting.

Preface

This dissertation is original, unpublished, independent work by the author, P. Gustainis.

Table of Contents

List of Tables

List of Figures

I would like to thank my supervisor Dr. Ian Affleck at the University of British Columbia. He has helped me throughout my research and assisted in the editing of this thesis. I would also like to thank Miles Stoudenmire for allowing me to use his DMRG software ITensor, and for helping me modify the simulation code to complete my research. I would like to thank Armin Rahmani for helping me during the start of my project and helping me get set up on the WestGrid cluster. I would also like to thank WestGrid for providing cluster time and troubleshooting resources so I could run my simulations successfully.

For my family, who have always believed in me.

1 Introduction

Quantum spin chains in one dimension (1D) are of great interest both theoretically and experimentally due to the enhancement of quantum effects that occur in 1D. Experimentally, they often provide very good models of quasi-1D solids with weak exchange interactions between chains [1]. Analytic predictions can be made about them using quantum field theory, including conformal field theory (CFT). Furthermore, they can be modeled using a variety of methods including density matrix renormalization group (DMRG) techniques. This numerical procedure, developed by Steve White in 1992 [3], is responsible for numerous advancements because it accurately and efficiently solves one dimensional quantum systems, and even some two dimensional systems.

The $S = 1$ Heisenberg antiferromagnetic chain,

$$H = \sum_j J\, \vec{S}_j \cdot \vec{S}_{j+1},\ J > 0$$

has been studied intensely both experimentally and theoretically since Haldane's discovery that there is an excitation gap (denoted Δ) from the ground state to a triplet of excited states, which is quite different from the $S = 1/2$ case which is gapless [4].

Further, the ground state of the system cannot be the Néel state, since continuous symmetries cannot be spontaneously broken in 1D, as was proven rigorously by the Mermin-Wagner-Coleman Theorem [5]. The ground state of the system, called the Haldane phase, has correlations and symmetries that are quite different from simple Néel order. It has full SO(3) symmetry that is robust to small symmetry breaking terms. In particular, this work studies a modified version of the famous Heisenberg antiferromagnetic spin chain for $S = 1$ spins in 1D with the following Hamiltonian,

$$H = \sum_j J\, \vec{S}_j \cdot \vec{S}_{j+1} + D\,(S_j^x)^2 + h\, S_j^z$$

This Hamiltonian is of interest since it used to describe many quasi-1D materials, which contain effective 1D chains with weak interchain coupling [1,15,16,17,18]. We neglect the interchain coupling in this study. We have modified the Heisenberg Hamiltonian with a crystal field splitting term $(S_j^x)^2$ which is a property of the material studied, and can in general have positive or negative sign depending

on the material. For this study, we focus on $D \leq 0$. In addition, we apply a magnetic field perpendicular to the crystal field, which can vary in magnitude, corresponding to coefficient h which will generally be considered to be positive ($h \geq 0$).

We study this quantum spin chain using DMRG methods to numerically simulate the spin chain. Since we consider a spin 1 chain with 3 states per site (thus the matrix that must be diagonalized is of size 3^L where L is the number of sites), exact diagonalization techniques are exhausted around $L = 20 - 30$ [6]. The correlation length ξ for the Heisenberg antiferromagnet has been estimated to be $\xi \sim 6$, thus we must use a more powerful numerical technique to obtain system sizes much larger than the correlation length [7]. DMRG can model systems with more than 100 sites with excellent accuracy and efficiency.

We are interested in a phase transition that occurs as we increase the magnetic field, where the symmetry of the Haldane phase is spontaneously broken. This phase transition is predicted to be in the Ising universality class for crystal field splitting $D < 0$ because the SO(3) symmetry is broken down to a Z(2) symmetry by the introduction of the crystal field term and magnetic field, and this symmetry is spontaneously broken at the critical point. We may use conformal field theory (CFT) to predict the spectra at the critical point for finite sized systems. As will be shown, the predicted finite size spectra corresponds to the numerical data quite closely, and can be used to accurately find the critical point. We also have quantum field theory predictions from Landau-Ginsburg theory that describe the system for small magnetic field [8]. One goal of this work will be the study the system as it goes from small fields, understood by Landau-Ginsburg, up to the critical field where the phase transition occurs, which is understood by CFT.

Electron-spin resonance (ESR) is an experimental technique used to probe the spectra of quantum systems by bombarding them with photons of an appropriate energy to excite electron spin flips in the material [9]. The absorption peaks indicate resonances where these transitions occur in the energy spectra. ESR has been used to study systems similar to the one studied in Ref. 5, and could be used to compare theoretical spectra and the spectra in materials to test correspondence with theoretical models. In quantum spin chains, spin flip excitations can be understood as transitions between different magnon states with the same momentum but energy that differs by the energy of the photon. By studying the momentum of excited states of our system, we can predict the excitations that would be detected by ESR on systems described by this model.

2 Background

2.1 Theory of Heisenberg antiferromagnet with no crystal field splitting (D=0)

First, we consider the Heisenberg antiferromagnet with only an external magnetic field applied,

$$H = \sum_j J\,\vec{S}_j \cdot \vec{S}_{j+1} + h\,S_j^z$$

This Hamiltonian conserves total spin in the z direction, $\langle S_{tot}^z \rangle$, which allows us to characterize states by their $\langle S_{tot}^z \rangle$ quantum number. This model Hamiltonian has been extensively studied, both using numerics as well as analytic techniques [7,10]. This system can be understood quite simply, since each state of the unperturbed Heisenberg antiferromagnet has a fixed $\langle S_{tot}^z \rangle$. When a magnetic field is applied, the states will Zeeman split according to their $\langle S_{tot}^z \rangle$. The ground state, in the Haldane phase, has $\langle S_{tot}^z \rangle = 0$, and the first triplet of single magnon excited states has $\langle S_{tot}^z \rangle = -1, 0, 1$ at energy $\Delta \approx 0.41J$ above the ground state. Thus, for positive h, the $\langle S_{tot}^z \rangle = -1$ state will meet the ground state energy at $h = \Delta$, and a phase transition occurs. In fact, it can be shown that the lowest energy two magnon state has energy 2Δ above the ground state, and minimum $\langle S_{tot}^z \rangle = -2$, and so on for higher number of magnon states [11]. Thus, at $h = \Delta$ we have a state of n magnons matching the ground state energy for every $n > 0$, $n \epsilon I$. This results in an effective Bose condensation of magnons in the 1D chain, as shown in Figure 1.

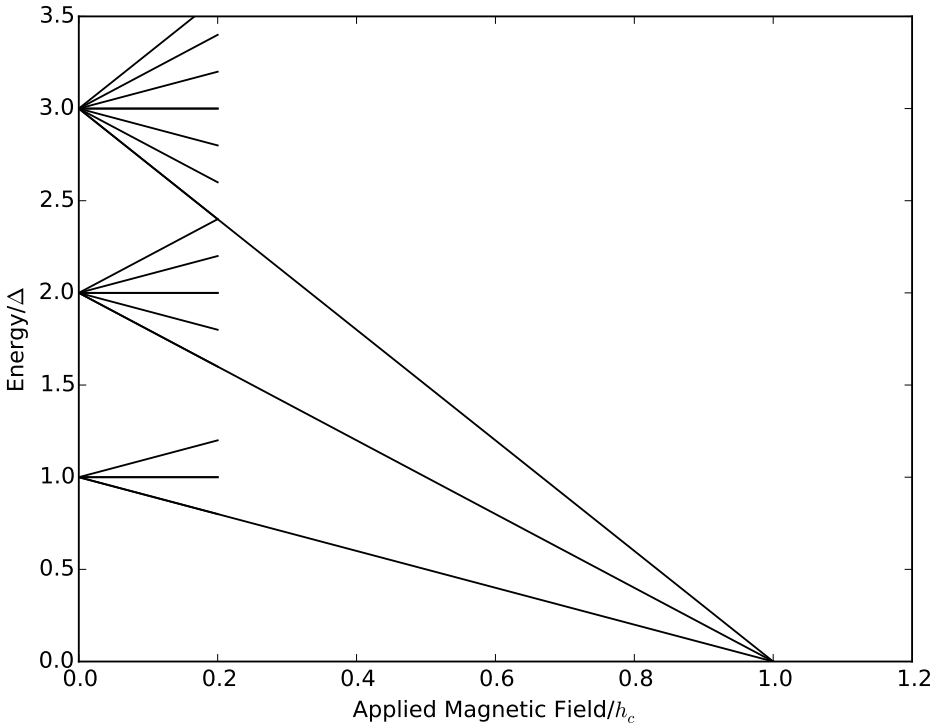

Figure 1: Schematic of Zeeman splitting
Theoretical expectation for the Zeeman splitting for each lowest energy multiplet up to S=3.

However, these magnons experience effective short range repulsive interactions [7]. At large distances, the short range interactions can be neglected and the magnons are effectively non-interacting. At short distances, these repulsive interactions act like the Pauli exclusion principle since the magnons do not want to be near to one another. For a small number of magnons in a large system (dilute) the magnons are seldom close together and the low energy spectrum is made up of states where these magnons are very far from one another, but cannot occupy the same state since there would be a strong repulsive interaction between them. This allows us to understand this condensate of magnons as a system of dilute non-relativistic non-interacting fermions [10]. This is valid for an arbitrarily weak repulsive interaction, as long as the intermagnon spacing is sufficiently large. Thus, our multimagnon state can be written as a sum of products of single, non-interacting fermion wavefunctions $\psi_i(x_j)$, multiplied by a sign function $\epsilon(x_1, x_2, ..., x_n)$ that changes the symmetry of the wavefunction from fermionic (antisymmetric) to bosonic (symmetric). The magnon wavefunction Ψ_M for n magnons can

be written as,

$$\Psi_M(x_1, x_2, ..., x_n) = \frac{1}{\sqrt{n!}}\epsilon(x_1, x_2, ..., x_n)\left[\sum_{P(i_1...i_n)}\prod_{i=1}^{n}\psi_1(x_{i_1})\psi_2(x_{i_2})...\psi_n(x_{i_n})sgnP\right]$$

where P denotes the permutation and $sgnP$ is the sign of the permutation. This fermionic wavefunction can be formed using the Slater determinant to guarantee antisymmetry in the wavefunction. Within the square brackets is our fermionic wavefunction, and the ϵ function outside corrects the fermionic symmetry to bosonic symmetry and $\frac{1}{\sqrt{n!}}$ normalizes the wavefunction.

Now it is quite elementary to calculate the energy of excited states at the point of condensation, for various numbers of magnons present, for a finite sized system. This can be used to directly compare with numerical results, and will serve as an excellent point of comparison for when we move to the Hamiltonian with crystal field splitting present. The energy of the magnon states is given by $E = \sum_{i=1}^{n} \frac{p_i^2}{2m}$, the energy for non-relativistic fermions at momentums p_i. The allowed values for p_i will be fixed by the allowed form of the wavefunction. We begin by imposing periodic boundary conditions on the system ($\Psi_M(0, x_2, ..., x_n) = \Psi_M(L, x_2, ..., x_n)$). However, for fermionic wavefunctions we must order the fermions by their relative position. Thus, when we move a particle from position 0 to L, we must permute $n-1$ times in our fermionic wavefunction, picking up a factor of $(-1)^{n-1} = sgnP$. So for an odd number of magnons, this does not give an overall sign change, and our individual wavefunctions have the form $\psi_i(x_j) = e^{\frac{2\pi i}{L}k_i x_j}$, $k_i = 0, \pm1, \pm2, ...$ The energy is simply $E = \frac{1}{2m}\left(\frac{2\pi}{L}\right)^2 \sum_{i=1}^{n}(k_i)^2$ since $p_i = \frac{2\pi}{L}k$, $k\epsilon I$. For an even number of magnons, we get an overall negative factor from the permutations ($sgnP = -1$). To resolve this and keep periodic boundary conditions for our Fermionic wavefunction, our individual wavefunctions will have the form $\psi_i(x_j) = e^{\frac{\pi i}{L}k_i x_j}$, $k_i = 0, \pm1, \pm2, ...$ Now, when we set $x_1 = L$ we get $\psi_i(L) = e^{\frac{\pi i}{L}k_i L} = -1$, which cancels with $sgnP = -1$, satisfying our periodic boundary conditions. The energy is given by $E = \frac{1}{2m}\sum_{k_i}\left(\frac{\pi k_i}{L}\right)^2 = \frac{1}{2m}\left(\frac{2\pi}{L}\right)^2 \sum_{i=1}^{n}\left(k_i + \frac{1}{2}\right)^2$ since $p_i = \frac{\pi}{L}k$, $k\epsilon I$. Now, we tabulate the lowest energy states for each n to develop our expected low energy spectrum,

Number of magnons	Energy $\div \frac{1}{2m}\left(\frac{2\pi}{L}\right)^2$	Momentum $\div \frac{2\pi}{L}$
$n=0$	$E=0$	$p=0$
$n=1$	$E=0,1,1,4,4,...$	$p-\pi=0,1,-1,2,-2,...$
$n=2$	$E=\frac{1}{2},2\frac{1}{2},2\frac{1}{2},..$	$p=0,1,-1,...$
$n=3$	$E=2,5,5,...$	$p-\pi=0,1,-1,2,-2,...$
$n=4$	$E=5,...$	$p=0,...$

Table 1: $D=0$ energy spectrum near critical point
Finite size spectrum for $D=0$ near the critical point calculated from non-interacting fermion model. Energies for the various states with fixed magnetization (number of magnons) and their corresponding momentum are included.

This gives the low energy spectrum at finite length: $E=\frac{1}{2m}\left(\frac{2\pi}{L}\right)^2\left(0,0,\frac{1}{2},1,1,2,2\frac{1}{2},2\frac{1}{2},...\right)$. It is important to note that the splitting of these levels goes as $\frac{1}{L^2}$ and even at finite length, the gap closes between the ground and first excited state at the critical point, then opens back up after the quantum critical point. A similar calculation is done in Ref. 7 for open boundary conditions.

For finite size systems, our theoretical picture of dilute interacting magnons begins to break down as we go to higher magnon states. This causes a slight deviation from the linear energy increase of multiplets at zero field with the number of magnons (i.e.$n\Delta \to n\Delta+\delta_n$). Therefore, at $h=\Delta$, we do not have all lowest energy magnon states condensing, only the $n=1$ magnon state for a finite system (since a single magnon cannot repulsively interact with itself). All other magnon states will cross the Haldane ground state at field $h=\Delta+\frac{\delta_n}{n}$, where δ_n will increase monotonically with n. This results in a cascading condensation where the ground state will continually increase in $\langle S^z_{tot}\rangle$as we increase field past the critical field. Before the phase transition, our ground state has $\langle S^z_{tot}\rangle=0$, with unbroken SO(3) symmetry, despite the Hamiltonian being reduced to SO(2) symmetry because of the magnetic field. After the critical point where the ground state possesses only SO(2) symmetry, we will have a uniform, integer $\langle S^z_{tot}\rangle$ that will increase with increasing field. Figure 2 shows a qualitative sketch of the ground state for the spin chain after the phase transition.

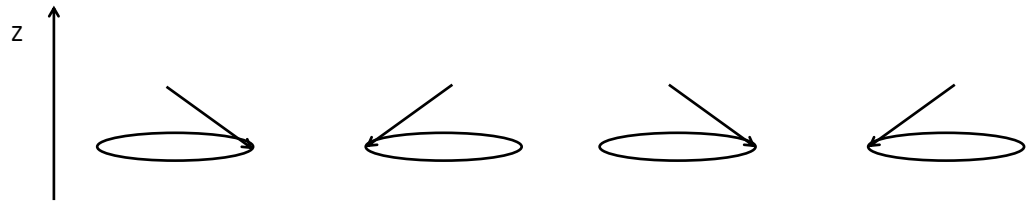

Figure 2: Sketch of $D = 0$ ground state after transition
Qualitative sketch of spins after critical point where SO(3) symmetry of the ground state goes to SO(2) symmetry and a magnetic moment appears. The spins have uniform moment in the z direction but have no preferred direction in the xy plane, characteristic of SO(2) symmetry.

In addition, predictions have been made about the momentum and energy dependence of excited states of the Heisenberg antiferromagnetic chain using the non-linear sigma model (NLSM) [11]. This model is exact only in the large S limit of our Hamiltonian and accurate near momentum $p = 0, \pi$, but provides at least a qualitative picture for the momentum of excited states that is verified by DMRG simulation.

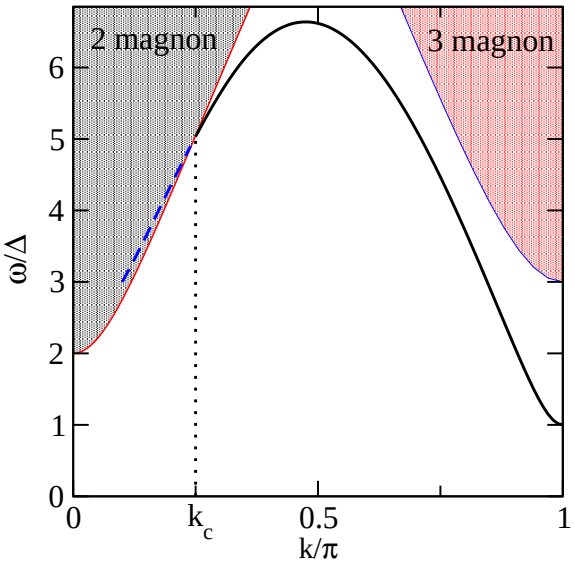

Figure 3: Schematic of excitation spectrum with momentum dependence
The above is a schematic of the excitation spectrum from Ref. 11 for states with 1, 2 and 3 magnons. The vertical axis indicates energy in units of the first excitation gap Δ and the horizontal axis is the crystal momentum in units of π. This is a reasonable qualitative sketch for our system if $D = 0$.

Figure 3 shows a schematic diagram of the spin chain excitation spectrum for $D = 0$. The solid

line indicates the one magnon spectrum, with lowest energy Δ at wave vector π. This line merges with the two magnon continuum, shown in grey, at some k_c. We also show the start of the 3 magnon continuum at wave vector π and energy 3Δ. Higher magnon continua are not shown on this plot but follow a similar pattern.

2.2 Theory of Heisenberg antiferromagnet with crystal field splitting

Now we consider the full Hamiltonian of interest,

$$H = \sum_j J\,\vec{S}_j \cdot \vec{S}_{j+1} + D\,(S_j^x)^2 + h\,S_j^z$$

First, we consider the quantum number for this Hamiltonian, which is different from before (conserved $\langle S_{tot}^z \rangle$). Taking the representation of $(S^x)^2$ in the canonical S^z basis for $S = 1$, we find,

$$(S^x)^2 = \tfrac{1}{2} \begin{pmatrix} 1 & 0 & 1 \\ 0 & 2 & 0 \\ 1 & 0 & 1 \end{pmatrix}$$

This now allows for transitions between local $S^z = 1$ and $S^z = -1$ states, meaning that we no longer conserve $\langle S_{tot}^z \rangle$, but can change between basis states of our Hamiltonian which differ in $\langle S_{tot}^z \rangle$ by 2. Now, we have total S^z parity (even/odd) to characterize our states. This makes our Hamiltonian block diagonal in these parity states. It is worth noting that $\langle S_{tot}^z \rangle$ can have any value for eigenstates of our Hamiltonian. Now the situation changes, because we can no longer think in terms of states with fixed magnetization. Further, the states in our spectrum do not Zeeman split as simply as before, since $\langle S_{tot}^z \rangle$ will change as we change magnetic field.

It is predicted that this transition will be in the Ising universality class because we are breaking the SO(3) symmetry of the Haldane phase into Z(2) ($S_j^x \to -S_j^x$) with our D term. The Z(2) symmetry is spontaneously broken at the critical point, as is characteristic for an Ising type transition (see Figure 4). We can now use conformal field theory, and conformal towers, to predict the finite size spectrum at the critical point using results from Cardy [13], and the Ising conformal structure from Di Francesco [14]. Note, we have dropped the constant in the energy formulae shown below since we only consider

energy differences between the ground state and excited states, and these constants cancel out when we take the difference.

Boundary Condition	Dimension	Parity	Energy
Periodic	$(0,0)(\frac{1}{2},\frac{1}{2})$ $(\frac{1}{16},\frac{1}{16})$	$Even\,(+)$ $Odd\,(-)$	$\frac{2\pi v}{L}\,(x_L + x_R)$
Free	0 $\frac{1}{2}$	$Even\,(+)$ $Odd\,(-)$	$\frac{\pi v}{L}x$

Table 2: Ising conformal tower structure
Above is shown the dimension of each conformal tower for periodic and free boundary conditions, including the parity of each conformal tower. In the final column is the formula for the energy of each state in the conformal tower. Information taken from Ref. 13.

We show calculations for free and periodic boundary conditions. From Cardy [13], we know the dimension of each conformal tower and what parity it has (shown in Table 2). For instance, our system with periodic boundary conditions (PBC) has three towers, two have even parity $(0,0), (\frac{1}{2},\frac{1}{2})$ and one has odd parity $(\frac{1}{16},\frac{1}{16})$. When a conformal tower has a pair of dimensions, as is the case for PBC, the energy is specified by a pair of numbers x_R and x_L, which come from a list of integers corresponding to their minimal character plus the dimension value. For example, for the $(\frac{1}{2},\frac{1}{2})$ conformal tower we look at the minimal character in the third row of Table 3 corresponding to $h_{r,s} = \frac{1}{2}$. The exponent of each q term tells us which integers are allowed, and the coefficients in front of each term tell us the degeneracy allowed. For example, the term q^2 appears so we are allowed the integer $a = 2$ but only one copy. Alternatively, the term $2q^4$ appears, so we are allowed two copies of the integer $a = 4$. The allowed pairs of (x_R, x_L) for this tower are given by $(\frac{1}{2}+a, \frac{1}{2}+a)$ where a is taken from the list of allowed integers for $h_{r,s} = \frac{1}{2}$, and $\frac{1}{2}$ comes from the dimension of the tower. So, the lowest energy pair allowed would be $(\frac{1}{2}+0, \frac{1}{2}+0)$ with energy $E = \frac{2\pi v}{L}(\frac{1}{2}+\frac{1}{2}) = \frac{\pi v}{L}(2)$. The next two states have $(x_R, x_L) = (\frac{1}{2}+1, \frac{1}{2}+0)$, $(\frac{1}{2}+0, \frac{1}{2}+1)$ with the same energy $E = \frac{2\pi v}{L}(\frac{1}{2}+\frac{3}{2}) = \frac{\pi v}{L}(4)$. For free boundaries, we have towers with a single dimension, not a pair of dimensions. The procedure is the same as shown above, only now we have a single x value instead of a pair, and a different formula for the energy.

Highest Weights for Ising Class ($h_{r,s}$)	Minimal Character	Allowed Integers a
$h_{1,1} = 0$	$1 + q^2 + q^3 + 2q^4 + 2q^5 + 3q^6 + ...$	$(0, 2, 3, 4, 4, 5, 5, 6, 6, 6, ...)$
$h_{1,2} = \frac{1}{2}$	$1 + q + q^2 + q^3 + 2q^4 + 2q^5 + 3q^6 + ...$	$(0, 1, 2, 3, 4, 4, 5, 5, 6, 6, 6, ...)$
$h_{2,1} = \frac{1}{16}$	$1 + q + q^2 + 2q^3 + 2q^4 + 3q^5 + 4q^6 + ...$	$(0, 1, 2, 3, 3, 4, 4, 5, 5, 5, 6, 6, 6, 6, ...)$

Table 3: Minimal character for each highest weight in Ising class
For the highest weights for each Ising class, we list the terms in the minimal character up to order 6, as well as the corresponding allowed integers used in the calculation of the energies of states in each conformal tower.

Now we may simply use the minimal characters for each of the highest weights with the formulae for the energy and tabulate the results in Table 4. We choose unique values/pairs of possible x values for each value/pair of highest weight(s). In the third column below we show the energies for each tower separately. In the fourth column, we order the energies from each tower, indicating their parity + or−, below each energy. This is what will be compared to numerical data obtained from DMRG.

Boundary Condition	Dimension	Energy (in units of $\frac{\pi v}{L}$)	Energy Spectrum (ordered, in units of $\frac{\pi v}{L}$)
Periodic	$(0,0)+$ $(\frac{1}{2},\frac{1}{2})+$ $(\frac{1}{16},\frac{1}{16})-$	$(0, 4, 4, 6, 6, ...)$ $(2, 4, 4, 6, 6, 6, ...)$ $(\frac{1}{4}, 2\frac{1}{4}, 2\frac{1}{4}, 4\frac{1}{4}, 4\frac{1}{4}, 4\frac{1}{4}, ...)$	$(0 \quad \frac{1}{4} \quad 2 \quad 2\frac{1}{4} \quad 2\frac{1}{4} \quad 4 \quad 4)$ $+ \quad - \quad + \quad - \quad - \quad + \quad +$
Free	$0+$ $\frac{1}{2}-$	$(0, 2, 3, 4, 4, ...)$ $(\frac{1}{2}, 1\frac{1}{2}, 2\frac{1}{2}, 3\frac{1}{2}, 4\frac{1}{2}, ...)$	$(0 \quad \frac{1}{2} \quad 1\frac{1}{2} \quad 2 \quad 2\frac{1}{2} \quad 3 \quad 3\frac{1}{2})$ $+ \quad - \quad - \quad + \quad - \quad + \quad -$

Table 4: Energy spectrum from conformal towers
For both periodic and free boundary conditions, we calculate the lowest energy states in each conformal tower. In the final column, we tabulate the lowest energy states from all conformal towers for each boundary condition, showing the corresponding parity below each state energy.

It is important to highlight that unlike the $D = 0$ case described before, we do not expect the gap to close for a finite system at the critical point. Instead, the gap will scale like $\frac{1}{L}$, and we will require conformal field theory predictions to find the critical point. Further, the ground state goes from unique to degenerate as the gap closes past the phase transition where the Z(2) symmetry is spontaneously broken. This is characteristic of an Ising transition. This is different from the $D = 0$ behavior, where the ground state goes from SO(3) symmetric to SO(2) symmetric as we go past the critical field. Figure 4 shows a sketch of the ground states of the system for $D < 0$ after the phase transition.

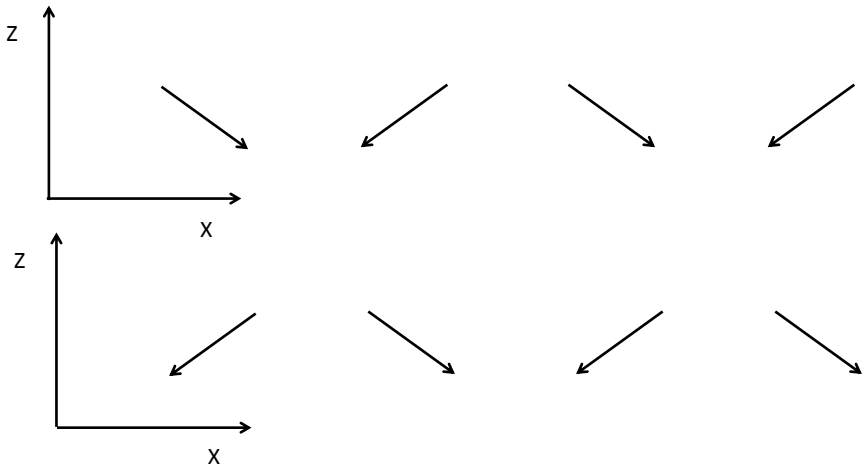

Figure 4: Sketch of $D < 0$ ground state after transition
Now spins have acquired overall magnetic moment, but also have a preferred alternating direction along the x axis. We have an degenerate ground states (both shown above) which can be mapped to one another by reversing each spin in the x direction. This shows that we have spontaneously broken the Z(2) symmetry after the phase transition, which is characteristic of an Ising phase transition.

2.3 Description of numerical simulation techniques

The primary numerical technique used in this study is Density Matrix Renormalization Group (DMRG) and we use the ITensor package designed by Miles Stoudenmire and Steven White [2]. DMRG is by far the most efficient and effective numerical technique for studying 1 dimensional quantum systems. It is however important to note that other numerical techniques were considered. For the $S = 1$ Heisenberg antiferromagnet, it has been shown that the correlation length of the system $\xi \sim 6$ [7]. We first tried using exact diagonalization techniques to study this system. However, working with $S = 1$ means our Hilbert space grows like $3^L$and makes it quite difficult to go past $L = 20 - 30$, which is still quite small compared to the correlation length of the system.

It is canonical to use open boundary conditions (OBC) when using DMRG, since the wavefunction Ansatz is generally in an OBC form. However, for our particular system we have a number of degenerate spin -$\frac{1}{2}$ edge states when we consider OBC. To see this, consider a similar spin-1 system in the Affleck-Kennedy-Lieb-Tasaki (AKLT) ground state [12].

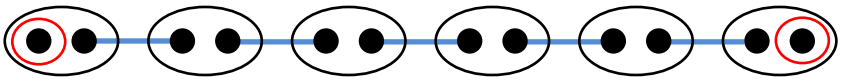

Figure 5: AKLT Ground state
The black dots are effective spin $\frac{1}{2}$'s, the black circles are the spin 1 sites, the blue lines are the singlet states, the red circles indicate the two unpaired effective spin-$\frac{1}{2}$'s.

When we join neighboring effective spin-$\frac{1}{2}$'s in singlets, we see that we have two unpaired spins at the ends of the chain for OBC. This creates four degenerate ground states at zero field, and will create up to four nearly degenerate states for each excited state as well. We observe similar edge states present in our system. Thus, to understand our system and its excited states using OBC DMRG, we would need up to four times as many excited states in our DMRG calculation as we would like to see in our study. This puts tremendous strain on the algorithm that struggles with larger numbers of excited states. Moreover, it is difficult to parse through all the excited states and determine which are edge state permutations of another state or constitute new bulk eigenstates.

Instead, we will consider periodic boundary conditions (PBC) for our DMRG simulation. This technique carries with it other difficulties because we are using an OBC Ansatz with a PBC Hamiltonian. This causes a large range interaction length for one hopping term that goes from site 1 to N that carries a large amount of entanglement entropy across all bonds in the DMRG algorithm. This increases computation time considerably, compared to OBC DMRG with the same number of sites, states and excited states desired. However, since we would need four times the excited states in OBC to study the same physics, this method is still much more efficient and allows us to study the bulk properties of our system far more easily.

Further, it will also allow us to measure the momentum of each state, which will be of great importance for making experimental predictions for electron spin resonance experiments. Consider the translation operator T which translates our wavefunction by one site. This operator will commute with the Hamiltonian for PBC $[T, H] = 0$. This means that for the eigenstates $|\psi_i\rangle$ of the Hamiltonian $H|\psi_i\rangle = E_i|\psi_i\rangle$ will also be eigenstates of T, $T|\psi_i\rangle = e^{ik_i a}|\psi_i\rangle$. Setting the lattice spacing $a = 1$, and

noting that due to PBC $T^N = I$, $k_i = \frac{2\pi n}{L}$, $n \epsilon Z$. The k_i can be associated with the crystal momentum of the state. We may now calculate momentum easily by taking a copy of our wavefunction, then shifting the tensor index label one site over for each local wavefunction $\langle\psi_i| T |\psi_i\rangle = \langle\psi_i| e^{ik_i a} |\psi_i\rangle = e^{ik_i a}$. Contracting the shifted state with the original wavefunction will give us the momentum of the state. This technique is only possible with PBC.

2.4 Theory of electron spin resonance

Electron Spin Resonance (ESR) is an experimental technique which uses photons to excite spin flips in a quantum system. The strength of the absorption signal from ESR is proportional to the imaginary part of the susceptibility $I(\omega) \propto \omega\chi''(\omega)$; where

$$2\hbar\chi''(\omega) = \left(1 - e^{-\hbar\omega/T}\right) \int_{-\infty}^{\infty} dt\, e^{i\omega t} \langle S^x_{tot}(t) S^x_{tot}(0)\rangle_T,\ S^x_{tot} = \sum_i S^x_i$$

where we have chosen the microwave field used to excite the spins polarized in the x direction [8]. In principle, the matrix element depends on the direction of the alternating field and could be in the y or z direction. In ESR experiments, we assume zero-momentum transitions since our Brillouin zone width should be much larger than the photon wavevector ($p = \frac{\hbar\omega}{v} = \frac{\hbar}{\lambda}$, where $v = c$ for the photon and $v_{crystal} \ll c$). Assume we have two states $|1, k_1\rangle, |2, k_2\rangle$ with energies, $E_1(k_1, h)$, $E_2(k_2, h)$ that can depend on momentum and applied magnetic field. Further, assume we have an allowed transition between these states at momentum k_0. Thus, $|E_1(k_0, h) - E_2(k_0, h)| = \omega\hbar$, and it can be shown [8],

$$2\hbar\chi''(\omega) = L\hbar\left(1 - e^{-\hbar\omega/T}\right) e^{-E_{min}(k_0,h)/T} \left|\partial E_1(k_0, h)/\partial k - \partial E_2(k_0, h)/\partial k\right|^{-1} \left|\langle 2, k_0| S^x_{tot} |1, k_0\rangle\right|^2,$$
$$E_{min} \equiv min\{E_1, E_2\}$$

Thus, to make predictions about the ESR peak intensity, we must be able to predict the matrix element between states as well as the momentum and field dependent dispersion relations of the two states $E_{1,2}(k, h)$. To do this theoretically we must use an approximate model. We model the first excited triplet of magnons in our system as a triplet of bosonic fields ϕ in the Landau-Ginsburg model, described by the Lagrangian,

$$\mathcal{L} = \frac{1}{2v}\left|\frac{\partial\phi}{\partial t} + \mathbf{h}\times\phi\right|^2 - \frac{v}{2}\left(\frac{\partial\phi}{dx}\right)^2 - \frac{1}{2v}\sum_i \Delta_i^2\phi_i^2$$

We solve the Euler-Lagrange equations for this field theory, fixing $\mathbf{h} = (0, 0, h)$, and obtain the field and momentum dependence energy dispersions for the three bosonic fields with k shifted by π,

$$\omega_3^2 = \Delta_3^2 + v^2k^2$$
$$\omega_{2,1}^2 = (\Delta_2^2 + \Delta_1^2 + 2v^2k^2)/2 + h^2 \pm [2h^2(\Delta_2^2 + \Delta_1^2 + 2v^2k^2) + (\Delta_2^2 - \Delta_1^2)/4]^{1/2}$$

The values of Δ_i are generally taken to be phenomenological parameters when comparing to experimental or numerical results. We will compare numerical results to these predictions.

2.5 Previous experimental results

There has been much experimental interest in quasi-1D materials with weak interchain coupling, since they are ideal for studying 1D quantum systems experimentally. One of the earlier examples of a quasi-1D S=1 antiferromagnetic material is $CsNiCl_3$[15,16]. Recently, another material $Ni(C_5H_{14}N_2)_2N_3(PF_6)$ (NDMAP) was found to also be in this class of materials [17], along with another material $Ni(C_2H_8N_2)_2NO_2ClO_4$ (NENP) [18]. For our study, we focus on the model compound $SrNi_2V_2O_8$ [1]. Using inelastic neutron scattering, the researchers in Ref. 1 estimated the effective crystal field splitting $\frac{D}{J} \approx -0.037$. In our investigation we will ignore interchain coupling and next-nearest neighbor interactions. This is an acceptable simplification since these couplings are measured to be 2 orders of magnitude smaller than the primary coupling J between nearest neighbors for $SrNi_2V_2O_8$.

3 Results

3.1 D = 0

We begin by showing results for our Hamiltonian in the case where $D = 0$. Though this system has been studied extensively both using numerical [7] and analytic techniques [10], we show new results for the system and reproduce a few older results. Further, it is a simple starting point for understanding the full behavior of the system with $D \neq 0$. We start with a quick overview of the low energy spectrum, then look at the rescaled spectrum near the critical point.

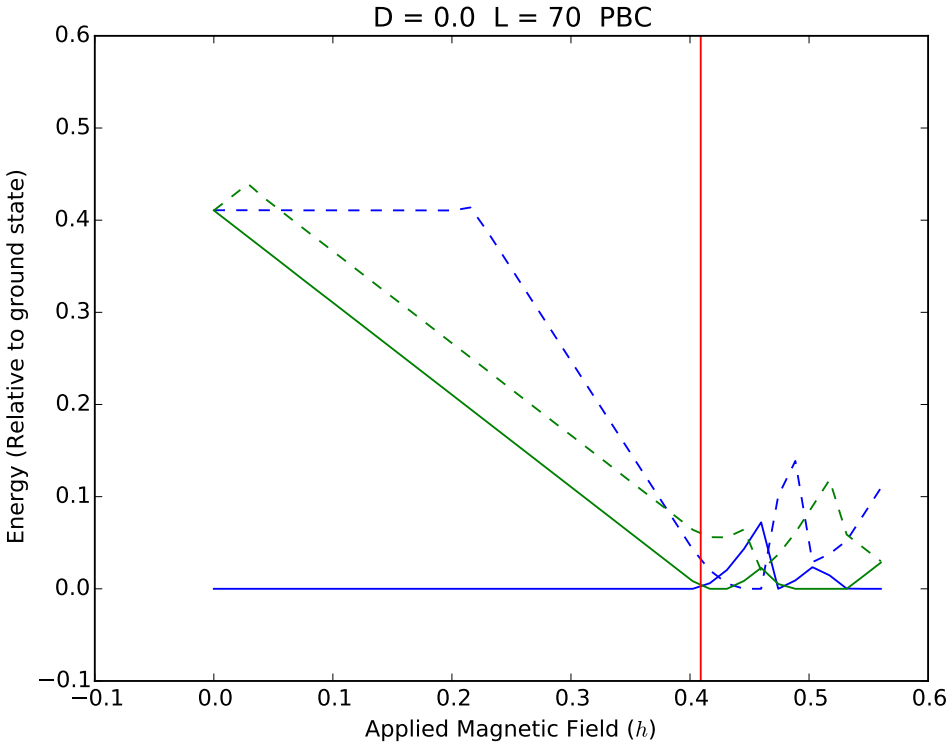

Figure 6: Energy Spectrum for $D = 0$
Blue lines indicate even parity states, green lines indicate odd parity states. We use the quantum numbers (parity) from $D \neq 0$ in our DMRG simulations for $D = 0$ because this will allow us to more easily compare graphs throughout the paper, though we could use S^z_{tot} quantum numbers for $D = 0$.

Figure 6 shows us the energy of excited states relative to the ground state. We see the excited triplet at energy $\Delta = 0.41$ that Zeeman splits with the applied magnetic field. We also observe there is another triplet above the first triplet with energy difference at zero field $\Delta E \approx \frac{v^2}{2\Delta}\left(\frac{2\pi}{L}\right)^2$. This expression comes from recognizing that in this PBC system, we are restricted to momentum $p = \frac{2\pi}{L}n$.

We then look at the spectral function from the NLSM and expand around momentum π in a relativistic approximation where $E = \sqrt{m^2v^4 + p^2v^2} \approx mv^2 + \frac{p^2}{2m}$, where now p is measured relative to momentum π. We identify the mass term $mv^2 = \Delta \to m = \frac{\Delta}{v^2}$ and we know $v \approx 2.49$ from a paper by I. Affleck and E. Sørensen [7]. This allows us to predict the gap between the triplets as $\Delta E \approx \frac{v^2}{2\Delta}\left(\frac{2\pi}{L}\right)^2 \approx \frac{298.5}{L^2}$. This shows us that there will be two copies of this second triplet at the same energy above the first triplet since we can have momentum $p = \pm\frac{2\pi}{L}$ (relative to π) that give the same energy.

Near the critical point at $h = \Delta$ (indicated by a vertical red line), we now see evidence of the cascading condensation in finite size systems. Notice the $S^z = -2$ state is at a gap δ from the ground states at the critical field. After the transition, the graph becomes very messy since we are measuring energy relative to the ground state, and now with the cascading transitions occurring, the ground state is changing to higher magnon states as we increase field.

We now study the system near the critical field and the behavior of the spectrum near this point.

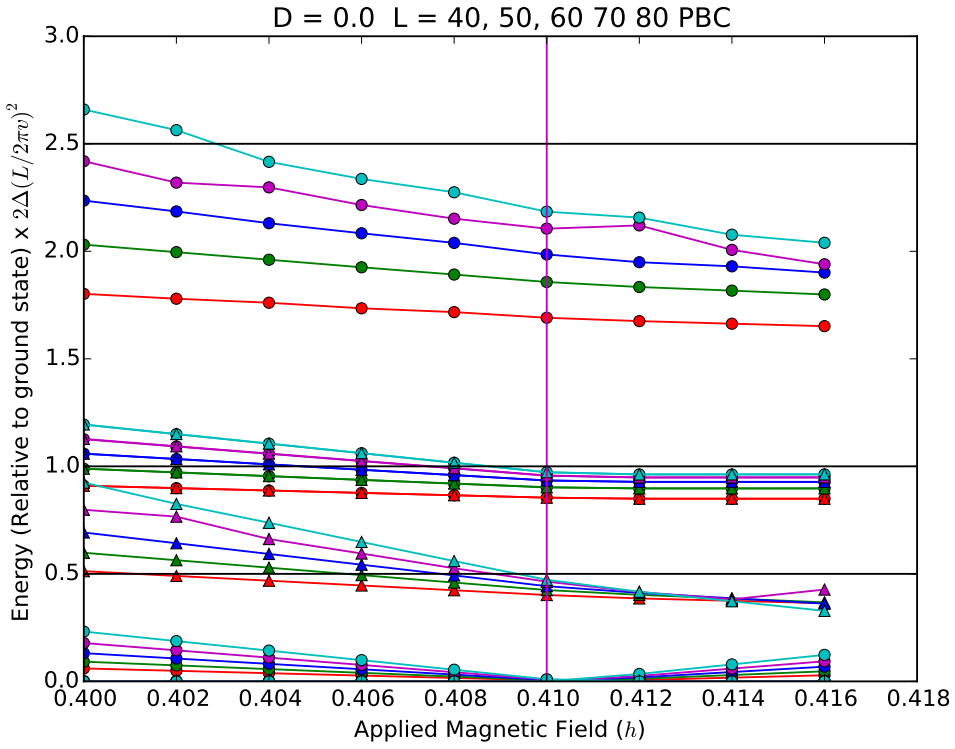

Figure 7: Rescaled spectrum for $D = 0$ near critical point
System size $L = 40, 50, 60, 70, 80$ are shown in red, green, blue, violet, light blue, respectively. The vertical purple line is the critical field at $h = \Delta = 0.41$. The black horizontal lines are the theoretical predictions from dilute repulsive bosons in 1D.

In Figure 7 we have taken DMRG data from system sizes $L = 40, 50, 60, 70, 80$ and plotted them on the same graph. We multiply each energy by the length of the system squared to remove the expected scaling behavior of the energies near the critical field, thus we expect that at the critical field all the field lines will converge on top of one another. We then use the predictions made before for the spectrum in units of $\frac{1}{2m}\left(\frac{2\pi}{L}\right)^2 = \frac{v^2}{2\Delta}\left(\frac{2\pi}{L}\right)^2$. The data follows the predicted spectrum well, particularly for lower energies. At higher energies where the magnon number is larger, there are likely interaction effects that are not accounted for in the theoretical model of dilute repulsive bosons, since we are working in systems with finite size. We would expect these deviations to decrease for larger system sizes. In fact, we see this clearly as our energy spectral lines approach the expected values as we increase the system size. Further evidence to support this interpretation is the increasing splitting as we go to higher magnon states. So long as we approach the theoretical prediction for increasing system size, it is consistent with our expectations.

Overall, this numerical evidence supports our theoretical predictions of finite size spectra near the critical point and we can easily match energy and momentum of each state to what was predicted. The differences between data and model can be easily explained by finite size effects and seem to converge to theoretical expectation as we go to larger system sizes.

3.2 D < 0

Experimentally, neutron scattering experiments can measure the coefficient of the crystal field splitting. The ratio of this coefficient D relative to the primary coupling J can vary dramatically from material to material, and can be positive or negative. We focus on negative D since this is what is observed for $SrNi_2V_2O_8$. We will first investigate a moderately large D relative to what was measured by Bera et al. The intention is to investigate the system in a regime that is dominated by the crystal field, where it is not a small perturbation on the system. However, we know from work done by Z.C. Gu and X.G. Wen [19] that there is a transition out of the Haldane phase at zero applied magnetic field h as we go to larger negative D. From the graph in their paper we can estimate that this transition occurs around $\frac{D}{J} \approx -0.3$ so we will choose $D = -0.2$ and investigate the phase transition as we increase the applied magnetic field. We start with an overview of the low energy spectrum, then consider the spectrum with additional excited states near zero applied field. Finally, we examine the rescaled spectrum near the critical field to compare with theoretical predictions.

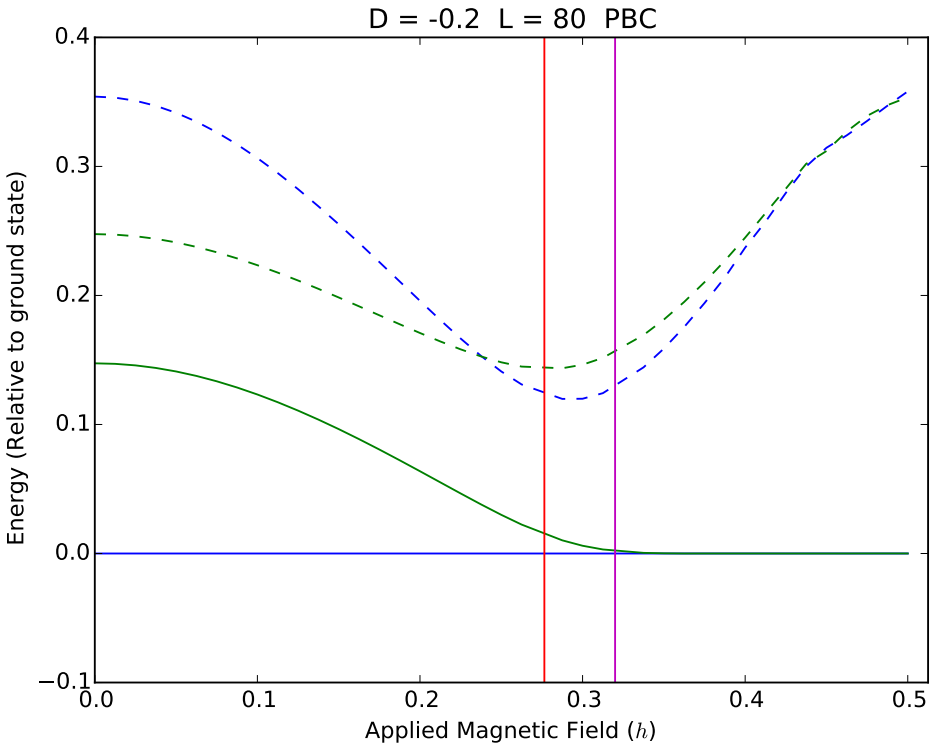

Figure 8: Energy spectrum for $D = -0.2$
Parity even states are shown in blue, parity odd in green. As can be seen, we have curves instead of straight lines as we increase our magnetic field. The vertical purple line is where the gap appears to close and we would expect the critical field is reached. However, the vertical red line is the transition field as predicted using CFT and finite size spectra (shown in Figure 10) which we assert is more accurate for the true infinite size transition field.

Comparing Figure 8 to the $D = 0$ data, we see a number of clear differences. Now, since magnon number is not a good quantum number, $\langle S^z_{tot} \rangle$ will change as we change the applied field. This results in curves which do not simply Zeeman split as we saw previously. We also see that the ground state and first excited state cross at a much smaller h_c, and become degenerate after the transition instead of crossing and splitting away from each other as compared to $D = 0$.

While many features of our system have changed drastically both quantitatively and qualitatively, we find parallels between the two systems that deepen our understanding and allow us to think in terms of our original picture with differences due to the crystal field splitting.

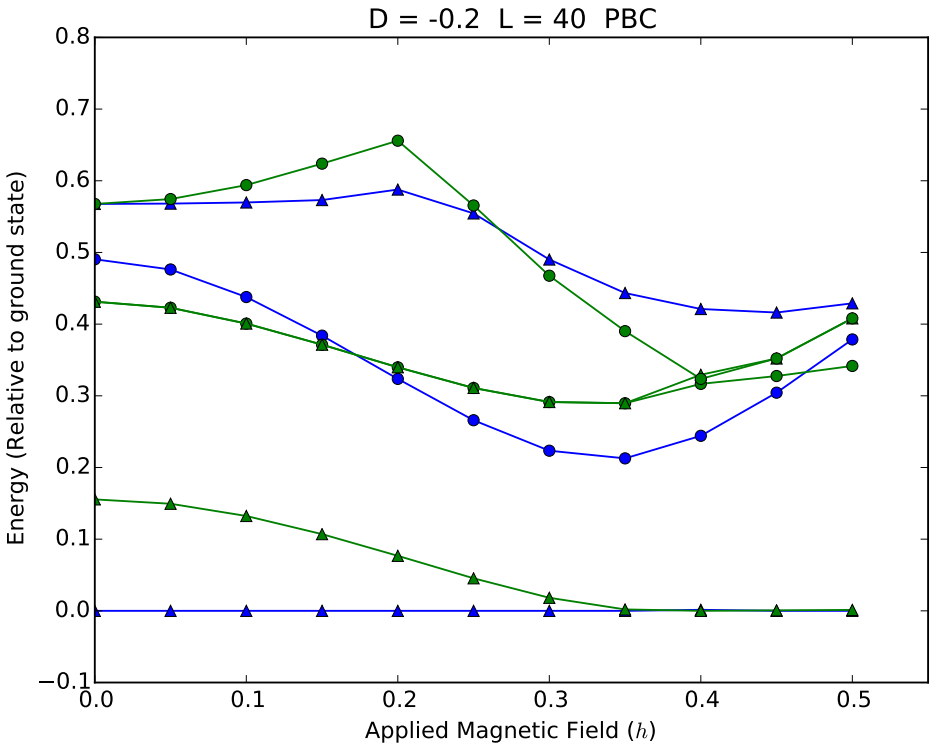

Figure 9: Energy spectrum for $D = -0.2$ for small system size
Numerous excited states are shown for parity even (in blue) and parity odd (in green)

As was shown in the background section, we predict the triplet to split into a singlet below Δ and doublet above the singlet. We study a small system to allow us to get many excited states from DMRG, shown in Figure 9. By measuring momentum using the method described before and measuring $\langle S^z_{tot} \rangle$ for each state, we can try to map these states to those seen in the $D = 0$ case with some perturbation caused by the crystal field splitting. Looking at the curves at zero field, the first state above the ground state is simply the bottom singlet from our triplet that has been split, with momentum $p = \pi$. The second green line is actually two data sets exactly on top of one another. These are the two singlets from two triplets at momentum $p = \pi \pm \frac{2\pi}{L}$, again split down similarly to the first excited state. Notice their curvature is quite similar to the curvature of the first excited state as well. The first blue line above the ground state has momentum $p = 0$, and near the middle of the curve, $\langle S^z_{tot} \rangle \approx -2$. This suggests that this is the bottom state from the $S = 2$ multiplet originally at energy $E_{h=0} = 2\Delta$ that has been split down by the large crystal field term. The next green and blue curve is the doublet (the other two states of the triplet) at momentum $p = \pi$, and are degenerate at zero field as expected.

These two states are intersected by higher energy states near field $h = 0.2$. The green curve at this point has momentum $p = \pi$, and $\langle S^z_{tot} \rangle \approx -3$, which suggests it is the bottom state from the $S = 3$ multiplet in the $D = 0$ picture, perturbed by crystal fields. The blue curve at this point is actually two curves with momentum $p = 0 \pm \frac{2\pi}{L}$ and $\langle S^z_{tot} \rangle \approx -2$. These are the higher momentum states for the $S = 2$ multiplet, analogous to what was seen for the $S = 1$ triplet.

Interpreting these states as perturbations of the original picture constructed for $D = 0$ is helpful so long as we keep clear that these states are related but not the same. Their magnetization varies with applied field, they have different quantum numbers, and are split from their original positions at zero applied magnetic field in the $D = 0$ diagram because of the crystal field. However, when we take these into account and measure the momentum of the states, we can clearly see how the crystal field changes our qualitative picture. This understanding will be useful when we consider much smaller $\frac{D}{J}$ as seen in $SrNi_2V_2O_8$.

Near the critical field, we will use CFT predictions developed beforehand and compare them to the spectra we obtain. Similar to the section before for $D = 0$, we will rescale our energies and plot the spectrum for multiple lengths to find the critical field where all these curves converge. However, we now rescale our energy by L instead of L^2.

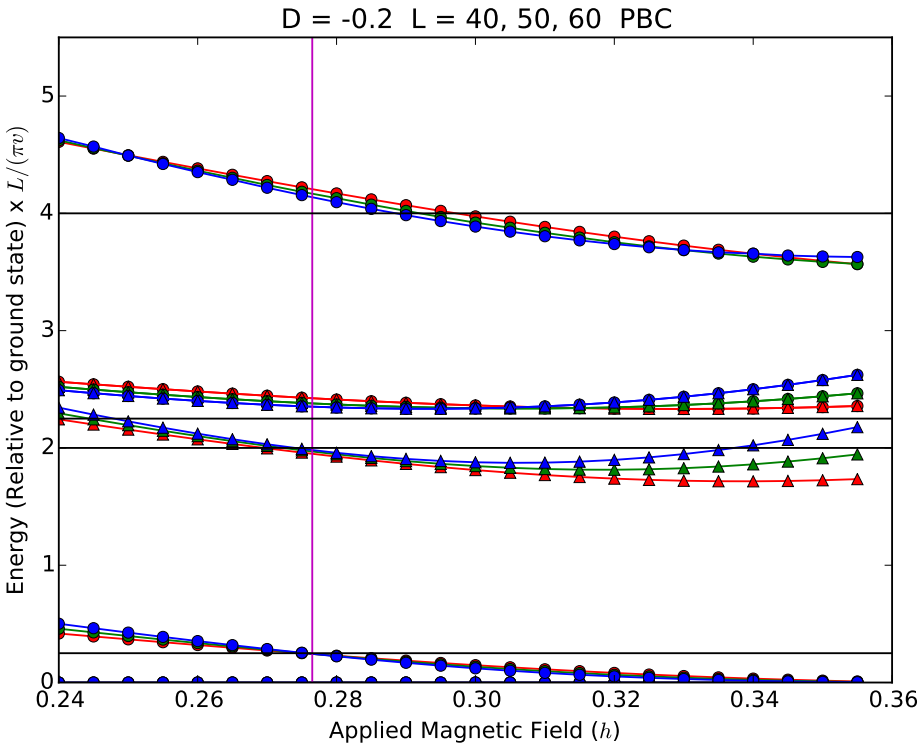

Figure 10: Rescaled spectrum for $D = -0.2$ near critical point
Red lines indicate data for $L = 40$, green lines for $L = 50$, and blue lines for $L = 60$. Vertical magenta line is the transition and the horizontal black lines show the theoretical predictions from CFT. Notice that for higher energy states we have a slight discrepancy between the theory and results. However, as we go to larger system sizes (red to green to blue) the data is moving towards the theoretical expectation at the critical field. We have used $v \approx 1.57$ to best fit the data.

In Figure 10, the curves seem to converge quite nicely near the critical field when rescaled appropriately, especially those with lower energies. An important difference between this plot and the one shown for $D = 0$, is that now we expect there to be a finite gap between the ground state and first excited state for a finite system. In the $D = 0$ system the gap closed at the same time as the energies converged, which meant either method of estimating the critical field gave similar results. Now the gap scales like $\frac{1}{L}$, and we can no longer estimate the critical field using the closing of the gap. Instead, CFT predictions give us a clear point at which the fields converge indicating the critical field. In theory, this convergence should happen for all excited states. However, this field theory is a low energy effective theory and begins to breakdown at higher energies. This breakdown should be resolved as we go to larger system sizes, and we can see in all the plots that there is a trend towards the expected energy scaling as we go to larger system sizes.

3.3 D $\lesssim$ 0

Now we consider a small negative crystal field splitting, which is what is expected for $SrNi_2V_2O_8$. We use the results from Bera et al. for the ratio $\frac{D}{J} \approx -0.037$. We shall see that in this regime the transition is driven primarily by the magnetic field, but many of the features from the crystal field dominated regime will persist. We start with an overview of the low energy spectrum, then consider our spectrum near zero field, comparing to Landau-Ginsburg theory. Finally, we examine the rescaled spectrum near the critical point.

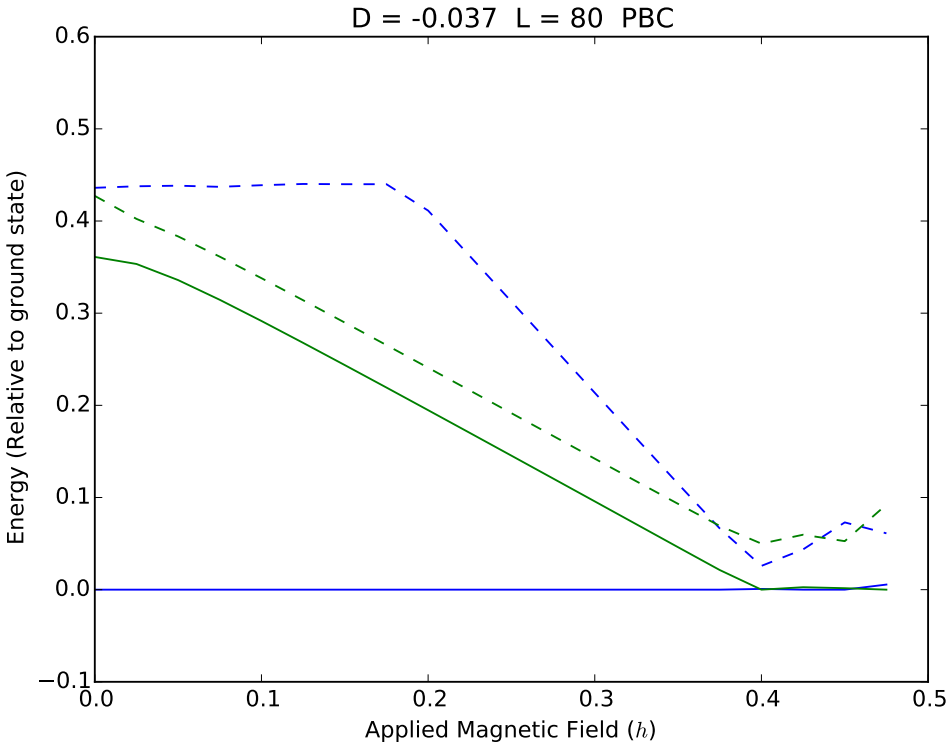

Figure 11: Energy spectrum for $D = -0.037$
The first two states for each parity for small negative crystal field splitting. Parity even states are shown in blue, parity odd in green.

It is insightful to compare and contrast Figure 11 with Figure 6 for $D = 0$. Past small fields but before the critical field, the graphs look almost indistinguishable qualitatively. We see the same 3 curves: the first being the bottom of the $S = 1$ triplet, the second being the same state at momentum $p = \pi \pm \frac{2\pi}{L}$, and the third being the $S^z = 0$ part of the triplet, that is intersected by the bottom state of the $S = 2$ multiplet. Notice that unlike the large D case, these spectral lines in the intermediate

region are almost perfectly straight with slopes corresponding to what would be expected for $D = 0$. The main differences are evident at fields near zero and above the critical field. Near zero field, the graphs are not straight lines as they are in $D = 0$. Instead, they have some curvature, and in fact start from $S^z_{tot} = 0$ at $h = 0$. This is to be expected since at zero field, the z direction is not preferred, but rather the x direction is preferred due to the crystal field. As we turn on the field in the z direction, the spins align to produce an overall moment in the z direction for certain states. This curvature is most evident for the first excited state as it curves from zero slope to a slope of -1. Further, around the critical point we see another change from the behavior of $D = 0$. The first excited state and the ground state merge and stay degenerate for all fields above the critical field. What's more, we do not see the same cascading condensation effect here as we saw in $D = 0$. In fact, since states are not constrained by an S^z_{tot} quantum number, they can have a magnetic moment that continually increases with increasing field. This results in a degenerate ground state that is not intersected by other excited states as field is increased, similar to the plots for large D.

Next we will look at our system near zero field and near the critical field since this is where our simple picture from D=0 does not work without modification.

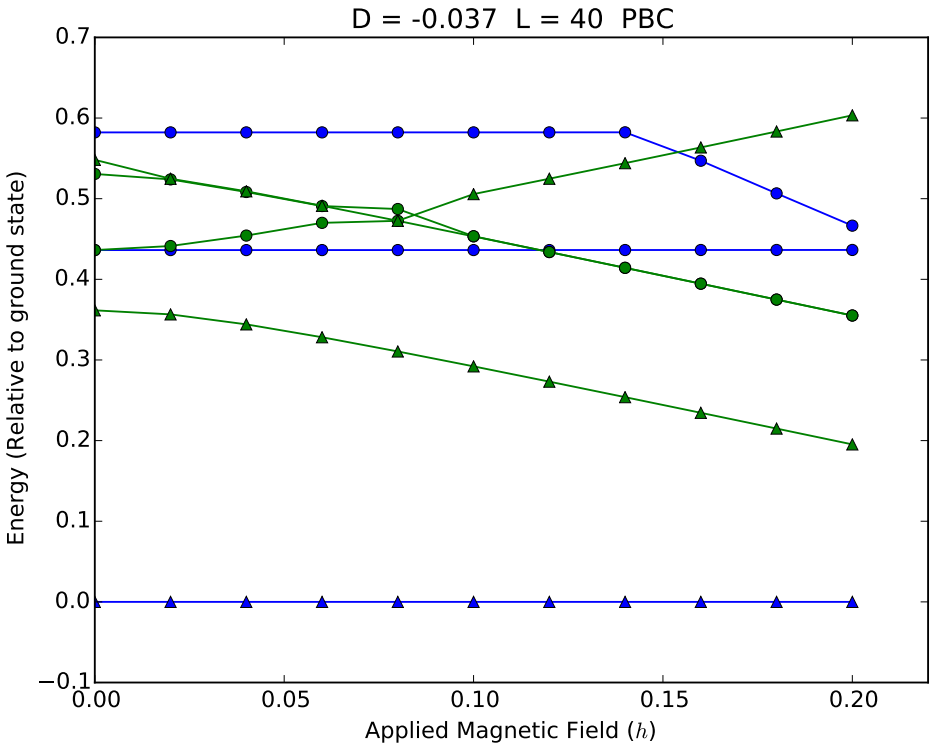

Figure 12: Energy spectrum for $D = -0.037$ near zero field
With a smaller system size, we may examine many more excited states. Using our understanding of how the spectrum changes with system size we can easily map this to larger system sizes which are harder to simulate with the same number of excited states. Parity even states are shown in blue, parity odd in green.

For small crystal field it is much easier to understand our spectrum as a modification of the D=0 system. In Figure 11 near zero field, the first 3 states are the first excited triplet from the D=0 system, but now the bottom state of the triplet has been split down as expected from our field theory predictions. The next two green lines are the bottom states from the triplets at momentum $p = \pi \pm \frac{2\pi}{L}$, that are degenerate as expected. The final blue lines are also degenerate and part of the triplet. At higher field, this final blue line is intersected by the bottom part of the $S = 2$ multiplet. The only large differences between this graph and the $D = 0$ graph seen before are the curvature near zero field and the splitting of the triplets at zero field.

We may now use the theory developed by I. Affleck for ESR spectra that should match our spectrum at small fields. We will fit using the energies at zero field. Notice the equations can be written entirely using variables $\alpha_i \equiv \Delta_i^2 + v^2k^2$, and h. Setting $h = 0$ we find $\omega_i^2 = \alpha_i$, allowing us to easily fit our

spectrum to theoretical predictions.

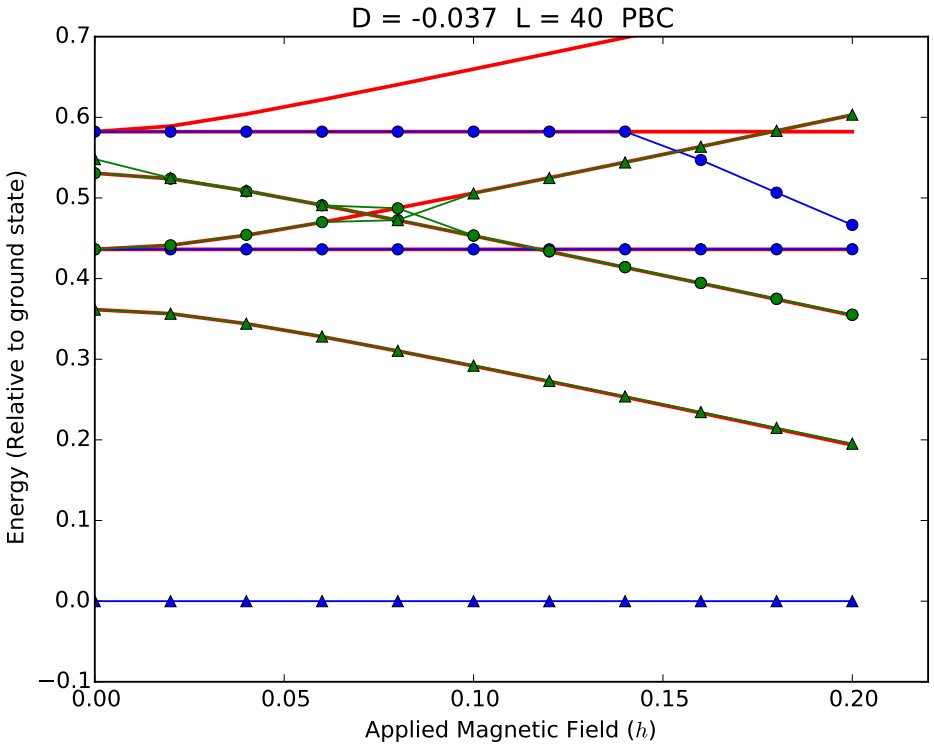

Figure 13: Energy spectrum for $D = -0.037$ near zero field with theoretical fits
The red lines are fits for both the lowest and next lowest triplet. Each fit lines corresponds to the data quite convincingly. The final red line trending upwards with no data matching it is the upper part of the higher momentum triplet, which was not captured by DMRG due to limited number of excited states. Parity even states are shown in blue, parity odd in green. $\Delta_1 = 0.36155$, $\Delta_2 = \Delta_3 = 0.43627$

In Figure 13, the red lines now indicate the fits obtained using the theory described beforehand. As we can see, the agreement is very good for fields in this range, and works well for the higher momentum triplet as well. We can use this theory to calculate the velocity for this system as well. Taking $\alpha_i^{\frac{2\pi}{L}} - \alpha_i^0 = v^2(\frac{2\pi}{L})^2$ (the superscript now indicates the momentum relative to π), we can calculate the velocity which has the value $v \approx 2.45$ for all branches, which is similar to the value $v \approx 2.49$ obtained by I. Affleck and E. Sørensen for $D = 0$ [7]. To see where this fit begins to breakdown we need to look closer to the critical field.

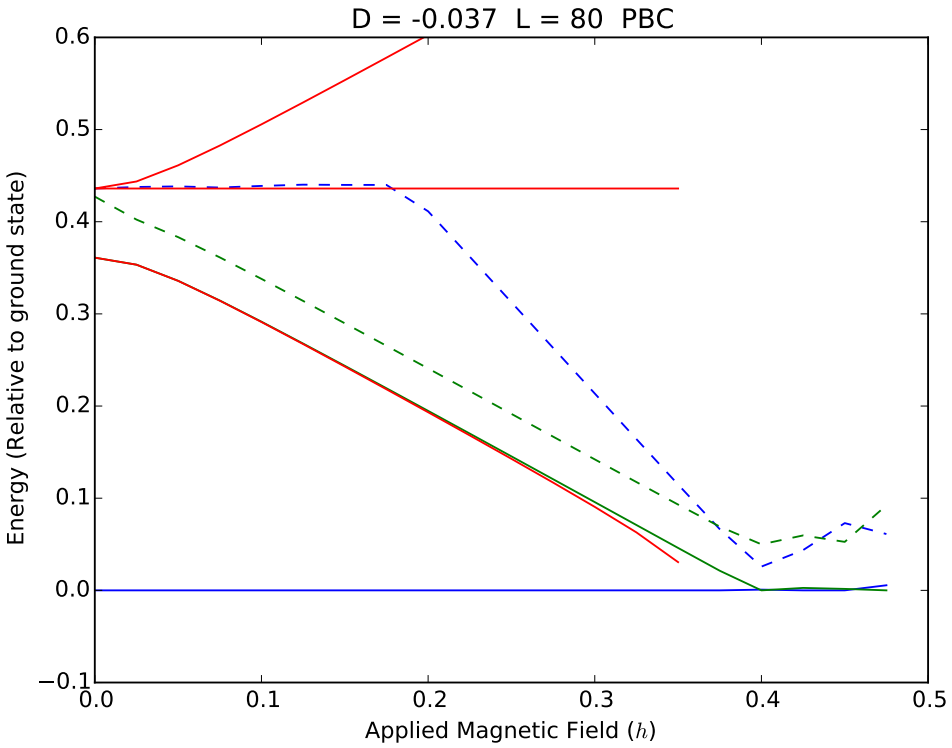

Figure 14: Energy spectrum for $D = -0.037$ with theoretical fits
We now go to a larger system size and look at only the first two excited states to evaluate the quality of the theoretical model for larger applied fields. We have used theoretical predictions and fit to our data (fits shown in red) and see excellent agreement between the two until we near the critical point. Again we are missing the upper part of the triplet because we have limited the number of excited states, though we still show the expected fit in red. Parity even states are shown in blue, parity odd in green. $\Delta_1 = 0.36102$, $\Delta_2 = \Delta_3 = 0.43604$

Figure 14 shows that the fit works quite well until very close to the transition for the first excited state, where it curves down too sharply before the transition. It is interesting to notice that for a small difference between $\alpha_1$and α_2 we simply get Zeeman splitting from the theory. Since the difference term in the square root can be neglected, $\alpha_1 + \alpha_2 \approx 2\alpha_1 \approx 2\alpha_2$ and we simplify into the form $\omega_{2,1}^2 = (\alpha_{2,1} \pm h)^2$. This is why for the intermediate region, where the curves look almost like Zeeman splitting, the fit works very well.

We use this theory for our previous $D = -0.2$ and see that theory breaks down much sooner for the first excited state.

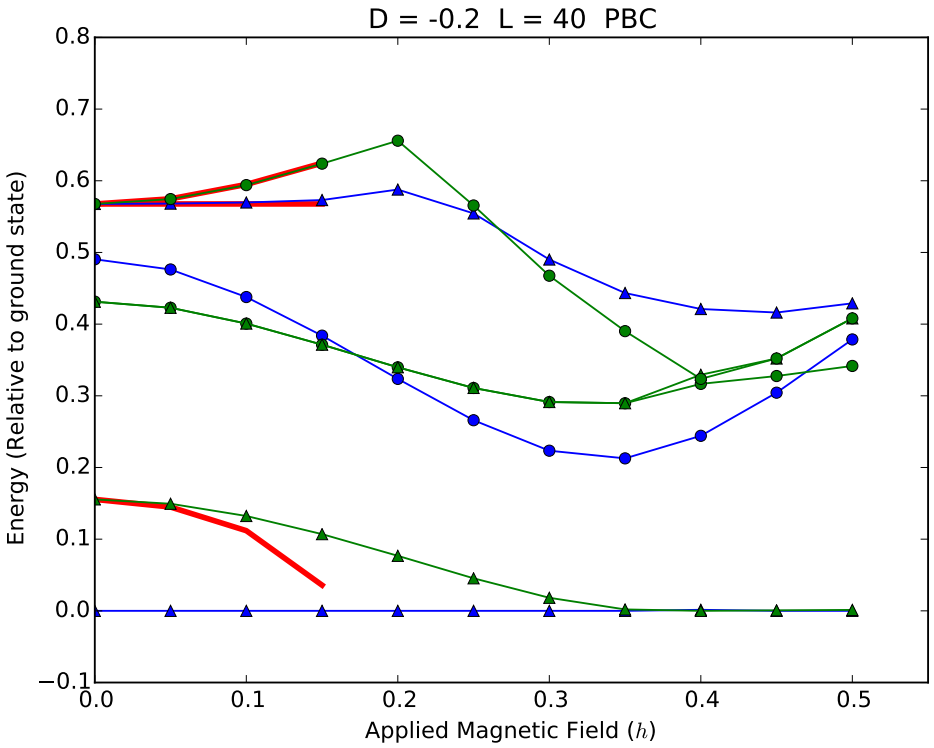

Figure 15: Energy spectrum for $D = -0.2$ with theoretical fits
The triplet is now split by a large amount, and the fits no longer match the data past small fields, particularly for the first excited state. The fits for the triplet states are shown in red. Parity even states are shown in blue, parity odd in green. $\Delta_1 = 0.15548$, $\Delta_2 = \Delta_3 = 0.56763$

To obtain the fits in Figure 15, we use the same fitting procedure described above, with fits in red for our triplet states. The fits for the upper two states in the triplet work quite well, though the fit for the lowest excited state quickly diverges from the data. This is not surprising since the theory developed only works for small applied fields. It also assumes the velocity of each state in the triplet is the same, which may not be the case any longer, and might be part of the reason for the large discrepancy in this case.

Finally, we consider the system near the critical point for multiple system sizes for $D = -0.037$. We would expect this system to have a finite size spectra that scales similarly to the spectrum for $D = -0.2$ near the critical point. So we rescale our energies by L and plot the energies for different length scales.

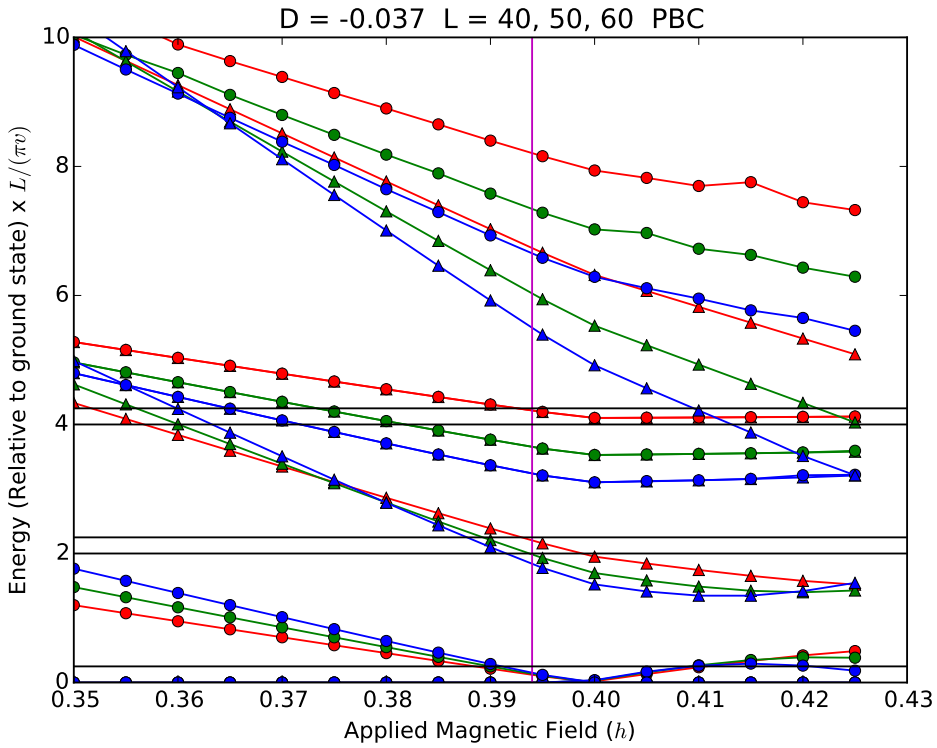

Figure 16: Ising-rescaled spectrum for $D = -0.037$ near critical field
We show $L = 40, 50, 60$ data in red, green and blue, respectively. The horizontal black lines are a best guess for the fit based on CFT predictions, but these should not be taken seriously. They are meant to show that our data is very far from Ising-like behavior near the critical point.

The spectrum in Figure 16 seems quite different from what was expected. First, the energies seem to converge as the first excited state and ground state become degenerate, which is more consistent with the spectrum for $D = 0$ near the critical point. Further, the spacing of the higher energy states do not follow the pattern we would expect for an Ising transition. Instead, we analyze the spectrum near the critical point using the methods for $D = 0$.

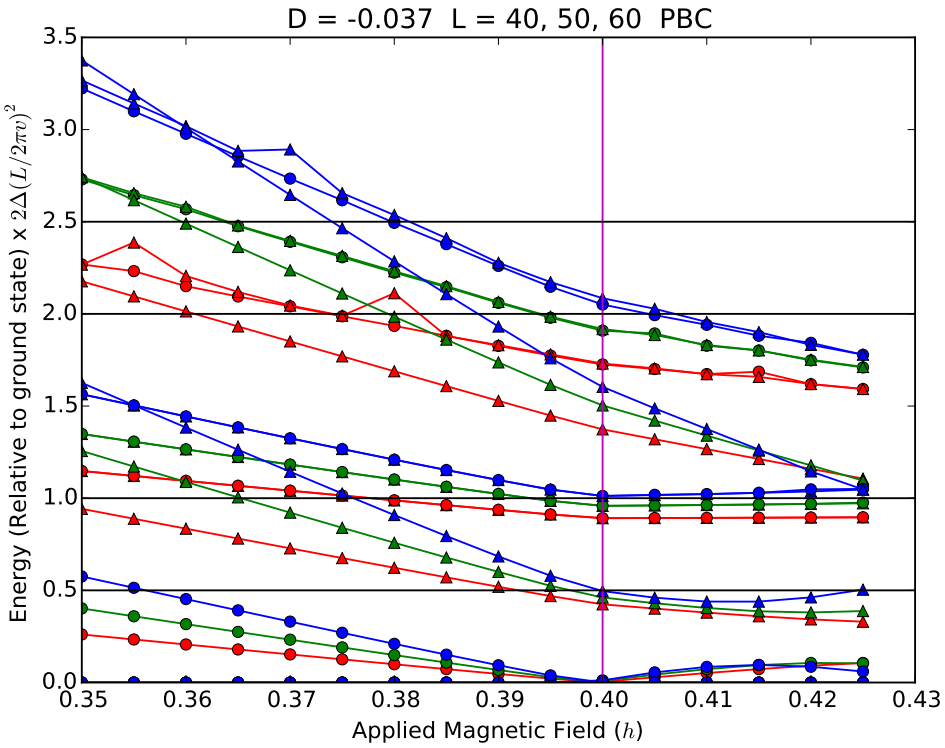

Figure 17: Condensation-Rescaled spectrum for $D = -0.037$ near critical field
We show $L = 40, 50, 60$ data in red, green and blue, respectively. Using the finite size spectrum for a Bose condensation transition, we can match our data to theoretical predictions, using the same velocity calculated before using Landau-Ginsburg theory fits ($v \approx 2.45$)

Surprisingly, in Figure 17 we see the spectrum at the transition is much more accurately described by this non-interacting fermion model instead of the Ising model. We suspect that this is because of finite size effects. If we consider the renormalization flow of the system near the critical point, we would expect that for small D and small system size we have not flowed far from the $D = 0$ system. For small D, we expect that we would see Ising like behavior as we increase our system size. However, the required system size is likely much larger than we can obtain using PBC DMRG for $\frac{D}{J} = -0.037$.

4 Conclusions

In this thesis, we examine the Heisenberg antiferromagnetic spin chain in 1 dimension with crystal field splitting and applied magnetic field terms using theoretical and numerical techniques. By first studying the system with zero crystal field splitting, we can characterize our system by thinking about states with different numbers of magnons present since we have conserved $\langle S^z_{tot} \rangle$. We use results from the non-linear sigma model (NLSM) to predict the structure of the excitation spectrum and how the excited states will behave when we apply a magnetic field. Near the critical point $h = \Delta$, we can map our system to non-interacting fermions in 1D and find a finite size spectra near the critical point which we compare to our numerical data. The data follows the theoretical predictions quite closely but deviate at higher energy, which corresponds to states with higher magnon numbers where our approximate mapping breaks down.

We then consider our system with a large negative crystal field splitting term $D < 0$. This term breaks $\langle S^z_{tot} \rangle$ conservation and we can no longer think in terms of states with a conserved number of magnons. This term also splits our excited multiplets at zero magnetic field, and the picture we obtain from the NLSM must be modified. At small field, we may use the Landau-Ginsburg model to approximate how the first excited triplet behaves as we increase from zero magnetic field. Near the critical field, we must now use conformal field theory to predict the finite size spectra for an Ising transition. We compare our theoretical predictions to numerical results obtained using DMRG and find good agreement near small and critical magnetic fields.

Finally, we study $\frac{D}{J} = -0.037$ which corresponds to experimental data obtained by Bera et al for $SrNi_2V_2O_8$ [1]. Here, the excitation spectrum exhibits qualitative elements from both the $D = 0$ and $D < 0$ excitation spectra. We would expect that near the critical point we would see behavior characteristic of an Ising transition, but when we examine the data, it more closely follows the non-interacting fermion model. This is likely because we are examining small system sizes as well as a small crystal field term, meaning that our renormalization flow is not far from the $D = 0$ system. For larger L at this fixed D we would expect to see Ising behavior near the critical point.

Bibliography

1. A.K. Bera, B. Lake, A.T.M.N. Islam, et al. Phys. Rev. B **91**, 144414 (2015)
2. Calculations were performed using the ITensor Library. http://itensor.org/
3. S.R. White, Phys. Rev. Lett. **69**, 2863 (1992); S.R. White, Phys. Rev. B **48**,10345 (1993)
4. F.D.M. Haldane, Phys. Rev. Lett. **50**, 1153 (1983)
5. N.D. Mermin and H. Wagner, Phys. Rev. Lett. **17**, 1133 (1966); S. Coleman, Comm. Math. Phys. **31**, 259 (1973)
6. T. Kennedy, Phys. Cond. Matt. **2**, 5737 (1990)
7. E.S. Sørensen and I. Affleck, Phys. Rev. Lett. **71**, 1633 (1993)
8. I. Affleck, Phys. Rev. B **46**, 9002 (1992)
9. J. Wertz, Electron spin resonance: elementary theory and practical applications. Springer Science and Business Media (2012)
10. I. Affleck, Phys. Rev. B **43**, 3215 (1991)
11. S.R. White and I. Affleck, Phys. Rev. B **77**, 134437 (2008)
12. I. Affleck, T. Kennedy, E.H. Lieb, H. Tasaki, Phys. Rev. Lett. **59**, 799 (1987)
13. J.L. Cardy, Nuc. Phys. B **275**, 200 (1986)
14. P. Di Francesco, P. Mathieu and D. Sénéchal, Conformal Field Theory, Springer-Verlag New York, (1997)
15. W.J.L. Buyers, et al. Phys. Rev. Lett. **56**, 371 (1986)
16. M. Enderle, K. Kakurai, K.N. Clausen, T. Inami, H. Tanaka and M. Steiner, Europhys. Lett. **25**, 717 (1994)
17. A. Zheludev, Y. Chen, C.L. Broholm, Z. Honda and K. Katsumata, Phys. Rev. B **63**, 104410 (2001)
18. J.P. Renard, M. Verdaguer, L.P. Regnault, W.A.C. Erkelens, J. Rossat-Mignod and W.G. Sterling, Europhys. Lett. **3**, 945 (1987)
19. Zheng-Cheng Gu and Xiao-Gang Wen, Phys. Rev. B **80**, 155131 (2009)